Active control of stick-slip torsional vibrations in drill-strings

Journal Title
XX(X):1–7

DOI: 10.1177/ToBeAssigned
www.sagepub.com/
SAGE

Thiago G Ritto[1] and Maryam Ghandchi-Tehrani[2]

Abstract

This paper presents active vibration control to reduce the stick-slip oscillations in drill-strings. A simplified two degree-of-freedom drill-string torsional model is considered. The nonlinear interaction between the rock and the bit is included in the model, where its parameters are fitted with field data from a 5km drill-string system. Different PD-control strategies are employed and compared, including the one that takes into account the weight-on-bit (axial force) and the bit speed. Optimization problems are proposed to obtain the values of the gain coefficients, and a torsional stability map for different weight-on-bit values and top-drive speeds is constructed. It is noted that the information of the dynamics at the bottom increases the performance of the PD-controller significantly in terms of the torsional vibration suppression, for the system analyzed.

Keywords

drill-string torsional dynamics, nonlinear dynamics, stability map, active control, stick-slip oscillations

Introduction

Excessive vibration of drill-strings is a concern for the oil industry. The vibrations are responsible, for instance, for fatigue of the structure and damage to the measurement equipment. This paper treats specifically torsional vibration control to reduce the stick-slip oscillation. There are many previous articles in the literature that have addressed the stick-slip phenomenon in drill-string vibration, and have made propositions for its control.

Concerning the nonlinear bit-rock interaction, Pavone and Desplans (1994) investigated the stick-slip phenomenon in drill-strings, and measurements of the bit-rock interaction are presented: bit rotational speed vs. torque on bit. A decaying exponential law is observed for this relationship. A nonlinear function is usually employed to model the bit-rock interaction (Khulief et al. (2007); Sampaio et al. (2007)).

Concerning control strategies, in Serranrens et al. (1998) a torsional vibration model with H-infinity control is developed. In Viguie et al. (2009) a torsional vibration model is controlled with a nonlinear passive targeted energy transfer. A lightweight is attached to the system and a nonlinear energy sink is created. In Kreuzer and Steidl (2012) torsional vibration is controlled by decomposing the drill-string dynamics into two traveling waves propagating in the direction of the top-drive and in the direction of the drill bit.

In Hiddabi et al. (2003) a coupled torsional-lateral model with a non-linear dynamic inversion control is developed. In Christoforou and Yigit (2003) a coupled model for axial-lateral-torsional vibrations using feedback control is considered. In Tucker and Wang (2009) a coupled model for axial-lateral-torsional vibrations (Cosserat theory) and feedback control strategies is analyzed. In Navarro-López and Cortés (2007) a torsional model controlled by sliding modes is developed. In Ritto et al. (2009a) a coupled axial-torsional model controlled by a fuzzy logic controller is analyzed. One can find a review on torsional control of drill-strings in Patil and Teodoriu (2013).

More recently, in Liu et al. (2014), a coupled axial-torsional model with state-dependent delay is considered. In Besselink et al. (2016), a feedback control strategy to mitigate torsional stick-slip oscillations using a coupled axial-torsional model for the drill-string is proposed.

Herein, we consider a torsional dynamical model, which is coupled with the axial force, known as weight-on-bit. For some given conditions, a pure torsional model is enough to represent the drill-string dynamics, as shown in Ritto et al. (2017). A simple 2-DOF system is chosen to focus the attention on the control strategies, as done by Jansen and van den Steen (1995); Leine et al. (2002); Christoforou and Yigit (2003); Richard et al. (2007). A more complete model with coupled axial-lateral-torsional vibrations can be found in Ritto et al. (2009b); Tucker and Wang (2009).

To assure that the applied torsional model analyzed in the present paper is representative, the field data from a 5km drill-string system presented in Ritto et al. (2017) is used to calibrate the nonlinear bit-rock interaction model and the response of the torsional model is compared with the field data bit speed. Measurement while drilling (MWD)

[1]Universidade Federal do Rio de Janeiro, Department of Mechanical Engineering, Brazil
[2]University of Southampton, Institute of Sound and Vibration Research, Southampton, UK

Corresponding author:
Thiago G Ritto, Universidade Federal do Rio de Janeiro Department of Mechanical Engineering, Rio de janeiro, 21941-450, RJ, Brazil.
Email: tritto@mecanica.ufrj.br

tools provide real-time and recorded data, and it helps understanding some downhole dynamics; Shi et al. (2016).

A PD-control strategy, which includes a control law for the weight-on-bit, was proposed in Monteiro and Trindade (2017). If we act on the axial force, the bit-rock interaction curve shifts, and stick-slip oscillations might be suppressed. One consequence is that an extra gain coefficient must be considered in the analysis. In this paper we follow a similar strategy proposed in Monteiro and Trindade (2017), but: (1) four PD-control strategies are compared with increasing parameters and information required, (2) optimization algorithms are applied to minimize cost functions and to obtain the control gain coefficients, and (3) the stability map (top-drive speed vs. weight-on-bit) is constructed for each control strategy.

Five control strategies are compared: (i) imposed top-drive speed, (ii) PD-control (2 gain coefficients) considering the response at the top, (iii) PD-control (3 gain coefficients) considering the response at the top and information about the weight-on-bit, (iv) PD-control (3 gain coefficients) considering the response at the top, information about the weight-on-bit, and the response at the bit, and (v) PD-control (5 gain coefficients) considering the response at the top, information about the weight-on-bit, and the response at the bit. The main goal of this paper is to construct the stability map for different strategies, and analyze how the stability region changes as more information is included in the control strategy.

The second section of this paper depicts the 2-DOF system considered in the analyses, as well as the control strategies employed. The third section presents the numerical results and, finally, the concluding remarks are made in the last section.

Formulation

Dynamical Model

The two degree-of-freedom (2DOF) drill-string torsional system sketched in Fig. 1 is considered. The degrees of freedom are θ_0 and θ_{bit}, which are the rotations of the top-drive and of the bottom-hole-assembly/bit. A control law is applied at the top-drive and a nonlinear bit-rock interaction torque occurs at the bottom of the column.

It is assumed that the bottom-hole-assembly (BHA) is a rigid body, and that the drill-pipe is flexible. The inertia and the natural frequency of the system are obtained calibrating the model with the field data found in Ritto et al. (2017). A linear model with linear viscous damping is considered for the column, but the bit-rock interaction is nonlinear. The equations of motion of the system are given by

$$\begin{aligned} I_0\ddot{\theta}_0 + k(\theta_0 - \theta_{bit}) + c(\dot{\theta}_0 - \dot{\theta}_{bit}) &= T_{top}\,, \\ I\ddot{\theta}_{bit} + k(\theta_{bit} - \theta_0) + c(\dot{\theta}_{bit} - \dot{\theta}_0) &= T_{bit}\,, \end{aligned} \tag{1}$$

where I_0 and I are the top-drive and drill-string moments o inertia, k is the drill-pipe stiffness, and c is the damping parameter. The torque at the top and the torque at the bit (Khulief et al. (2007); Sampaio et al. (2007); Ritto et al. (2017)) are

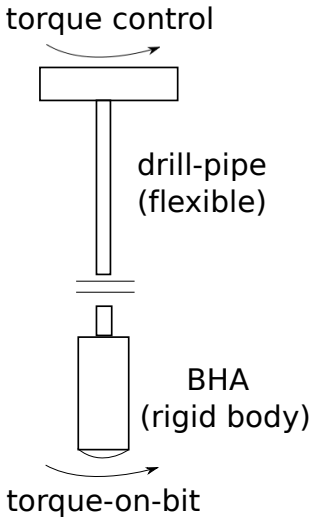

Figure 1. Sketch of a drill-string.

$$\begin{aligned} T_{top} &= T_{control}\,, \\ T_{bit} &= -b_0\left(\tanh(b_1\dot{\theta}_{bit}) + \frac{b_2\dot{\theta}_{bit}}{1+b_3\dot{\theta}_{bit}^2}\right). \end{aligned} \tag{2}$$

in which the torque is given in [N.m] and $\dot{\theta}_{bit}$ in [rad/s]. The parameters of the nonlinear bit-rock interaction model are positive constants b_0 [N.m], b_1 [s], b_2 [s], b_3 [s^2], and they depend on the weight-on-bit, rock properties and cutting characteristics. We can write $b_0 = \bar{r}\mathcal{W}$, where $\mathcal{W}$ is the weight-on-bit and $\bar{r}$ is the bit effective radius. Figure 2 shows the nonlinear bit-rock interaction, where the fitted model is compared with the available field data presented in Ritto et al. (2017). Although the fluctuation of the field data is big, the fitted bit-rock interaction model is in good agreement with the experiments.

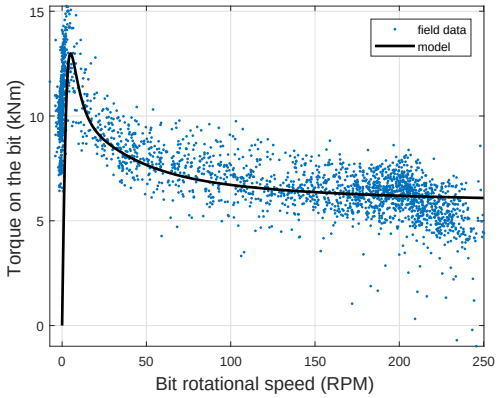

Figure 2. Torque applied to the bit: field data (Ritto et al. (2017)) vs. fitted model.

The state space model is given by:

$$\dot{\mathbf{y}} = \begin{bmatrix} \mathbf{0} & \mathbf{I} \\ -\mathbf{M}^{-1}\mathbf{K} & -\mathbf{M}^{-1}\mathbf{C} \end{bmatrix}\mathbf{y} + \begin{bmatrix} \mathbf{0} \\ \mathbf{M}^{-1}\mathbf{T}(\mathbf{y}) \end{bmatrix}, \tag{3}$$

where $\mathbf{y} = (\theta_o, \theta_{bit}, \dot{\theta}_o, \dot{\theta}_{bit})$, $\mathbf{I}$ is the two by two identity matrix, $\mathbf{0}$ is the zero matrix (or vector). The other matrices and vectors are given by

$$\mathbf{M} = \begin{bmatrix} I_0 & 0 \\ 0 & I \end{bmatrix} \quad , \quad \mathbf{C} = \begin{bmatrix} c & -c \\ -c & c \end{bmatrix} \quad , \tag{4}$$

$$\mathbf{K} = \begin{bmatrix} k & -k \\ -k & k \end{bmatrix} \, , \quad \mathbf{T}(\mathbf{y}) = \begin{bmatrix} T_{top} \\ T_{bit} \end{bmatrix} \, . \tag{5}$$

Note that linear models are assumed for stiffness and viscous damping; the nonlinearity comes only from the bit-rock interaction T_{bit}. It should be remarked that a second damping parameter could be added directly to the BHA, which would decrease a rigid body rotation. However, for the purpose of the present analysis, this parameter is not important, and it would be another parameter to be identified.

Control strategies

If the motor at the top (top-drive) can sustain a constant speed ω_{ref}, i.e., the drive torque assumes any value necessary to maintain the reference speed, then only one equation must be solved:

$$I\ddot{\theta}_{bit} + k(\theta_{bit} - \omega_{ref} t) + c(\dot{\theta}_{bit} - \omega_{ref}) = T_{bit} \, . \tag{6}$$

When the PD-control is applied, the control gain coefficients $\mathbf{k}$ are obtained solving an optimization problem, where an objective function should be minimized. That is, for each pair $\{\omega_{ref}^{(i)}, \mathcal{W}_{ref}^{(j)}\}$, $\{i = 1, 2, .., n\}$, $\{j = 1, 2, .., m\}$, an optimization problem is solved to compute the optimal gain coefficients, as shown in Eq. 7

$$\mathbf{k}^* = \text{argmin} \quad J(\mathbf{k}) \, , \tag{7}$$

where $\mathbf{k}$ belongs to an admissible space and J is the cost function defined in the next sections, which depends on the system response.

The stick-slip severity factor is defined by $SSS = (\omega_{max} - \omega_{min})/(2\omega_{ref})$. This is how we interpret this factor. If the bit speed reaches a constant speed, which is equal to the reference speed at the top, this factor is equal to zero and the system is stable. If there is a limit cycle oscillation for the bit speed, this factor is greater than zero, and the system is considered to be unstable.

Control strategy 1 : the first control strategy adopted is the following one

$$T_{top}(\theta_0) = k_P(\omega_{ref} t - \theta_0) + k_D(\omega_{ref} - \dot{\theta}_0) \, , \tag{8}$$

with control gain coefficients $\mathbf{k} = (k_P, k_D)$ and ω_{ref} as the reference speed at the top-drive. In this strategy the cost function is defined as

$$J(\mathbf{k}) = ||\omega_{ref} - \dot{\theta}_0(\mathbf{k})|| \, , \tag{9}$$

which means that the goal is to obtain $\mathbf{k}$ such that the top-drive speed is as close as possible to the reference speed. Note that only information at the top is taken into account, i.e., θ_0 and $\dot{\theta}_0$.

Control strategy 2 : the second control strategy adopted is similar to the one proposed by Monteiro and Trindade (2017), where the weight-on-bit is also included in the control law, such that the bit-rock interaction curve can be changed. Note that the axial force at the top (weight-on-hook) is directly related to the axial force at the bottom (weight-on-bit).

$$\begin{aligned} T_{top}(\theta_0) &= k_P(\omega_{ref} t - \theta_0) + k_D(\omega_{ref} - \dot{\theta}_0) \, , \\ \mathcal{W} &= \mathcal{W}_{ref} + k_{\mathcal{W}}(\dot{\theta}_0 - \omega_{ref}) \, . \end{aligned} \tag{10}$$

The control gain coefficients are $\mathbf{k} = (k_P, k_D, k_{\mathcal{W}})$, and $k_{\mathcal{W}}$ is limited so that the actual weight-on-bit variations are smaller than 20%. As explained in Monteiro and Trindade (2017) "Therefore, if the angular velocity is larger than the reference one, the weight-on-bit is increased relative to the target one (which allows higher rate of penetration). But, in the opposite case, where the angular velocity is smaller than the target one, meaning that stick-slip is potentially occurring, the weight-on-bit is reduced to alleviate the frictional reaction torque."

We propose to obtain the control gain coefficients using the same cost function of the previous strategy,

$$J(\mathbf{k}) = ||\omega_{ref} - \dot{\theta}_0(\mathbf{k})|| \, . \tag{11}$$

As in the strategy 1, only information at the top is taken into account, i.e., θ_0, $\dot{\theta}_0$ and weight-on-hook (directly related to the weight-on-bit).

Control strategy 3 : the third control strategy adopted is again similar to the one proposed by Monteiro and Trindade (2017). However, now information from the bottom is needed to implement this strategy. Note that $\dot{\theta}_{bit}$ appears in the second equation below.

$$\begin{aligned} T_{top}(\theta_0) &= k_P(\omega_{ref} t - \theta_0) + k_D(\omega_{ref} - \dot{\theta}_0) \, , \\ \mathcal{W} &= \mathcal{W}_{ref} + k_{\mathcal{W}}(\dot{\theta}_{bit} - \omega_{ref}) \, . \end{aligned} \tag{12}$$

The control gain coefficients are $\mathbf{k} = (k_P, k_D, k_{\mathcal{W}})$. For this strategy a multi-objective cost function is proposed, to include the bit dynamics, $\dot{\theta}_{bit}$

$$J(\mathbf{k}) = ||\omega_{ref} - \dot{\theta}_0(\mathbf{k})|| + (\omega_{bit}^{max}(\mathbf{k}) - \omega_{bit}^{min}(\mathbf{k})) \, , \tag{13}$$

which means that there are two goals put together: (1) obtain $\mathbf{k}$ such that the top-drive speed is as close as possible to the reference speed and (2) the bit oscillations are as small as possible.

It should be remarked that usually, in the field, this information is not available, but we want to investigate how much the control strategy would improve if this information was available. And, also, an observer can be constructed to estimate $\dot{\theta}_{bit}$.

Control strategy 4 : the fourth control strategy which is proposed in the present paper is similar to the strategy 3, nevertheless it considers the bit speed in the control law of the torque. Doing so we reinforce the main objective, which is to reduce the torsional vibration of the system.

$$\begin{aligned} &T_{top}(\theta_0) = k_{P1}(\omega_{ref}t - \theta_0) + k_{P2}(\omega_{ref}t - \theta_{bit}) \\ &+k_{D1}(\omega_{ref} - \dot{\theta}_0) + k_{D2}(\omega_{ref} - \dot{\theta}_{bit}) \,, \\ &\mathcal{W} = \mathcal{W}_{ref} + k_{\mathcal{W}}(\dot{\theta}_{bit} - \omega_{ref}) \,. \end{aligned} \tag{14}$$

The control gain coefficients are $\mathbf{k} = (k_{P1}, k_{P2}, k_{D1}, k_{D2}, k_{\mathcal{W}})$. The cost function is the same one used in the previous strategy

$$J(\mathbf{k}) = ||\omega_{ref} - \dot{\theta}_0(\mathbf{k})|| + (\omega_{bit}^{max}(\mathbf{k}) - \omega_{bit}^{min}(\mathbf{k})) \,. \tag{15}$$

Numerical results

The feedback control gain coefficients are constraint to $k_P \in [0, 10^5]$, $k_D \in [0, 10^3]$, and $k_{\mathcal{W}}$ is limited so that the actual weight-on-bit variations are smaller than 20%. To compute the gain coefficients, optimization is carried out using an interior-point algorithm, and the system dynamics is computed with the Runge-Kutta integration scheme.

The following system were obtained, calibrated with the available field data in Ritto et al. (2017): $\omega_n = 0.85$ [rad/s] (natural frequency), $\xi = 0.25$ (damping ratio), $I = 383$ [kg.m^2], $I_0 = 9.58$ [kg.m^2], $b_0 = 5671$, $b_1 = 0.4775$, $b_2 = 8.7854$, $b_3 = 4.5595$. The bit-rock interaction parameters were obtained for $\mathcal{W}$ equals to 245 kN. Assuming that T_{bit} is linear with respect to the weight-on-bit, a coefficient is used to multiply T_{bit} such that different values of $\mathcal{W}$ can be simulated. For example, if the $\mathcal{W}$ is 200 kN, then T_{bit} must be multiplied by $200/245 = 0.816$.

Figure 3 shows the bit rotational speed obtained integrating Eq. (6) with top-drive speed 120 RPM and $\mathcal{W}_{ref}$ equals to 245 kN. The computational model response is compared with the available field data (Ritto et al. (2017)). The model is not perfect, but it performed very well to capture the stick-slip oscillations, with amplitude and frequency of oscillation in the same order of magnitude of the field data signal. Recalling that a 1DOF system is being used to represent a 5km drill-string system.

Figure 4 shows the bit rotational speed obtained from integrating Eq. (6) for three different top-drive speeds: 60 RPM, 100 RPM and 140 RPM. Depending on the top-drive speed the response have different amplitudes torsional oscillation (and different frequency of oscillation), or it can simply not oscillate. The corresponding SSS values are 1.66, 1.22, and 0.02. The value of SSS decreases with increasing top-drive speeds.

Usually for higher speeds the system escapes from the stick-slip condition, i.e., the bit speed is equal to the top-drive speed. A similar analysis can be done with respect to the weight-on-bit, but on a different sense. Usually for lower weight-on-bit the system escapes from the stick-slip condition.

In the sequence, stability maps are constructed, varying the top-drive speed ω_{ref} and the weight-on-bit $\mathcal{W}_{ref}$, for the

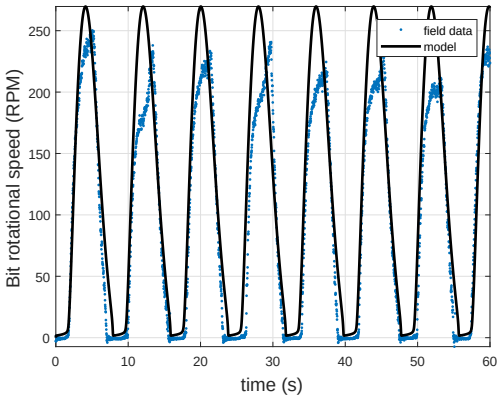

Figure 3. Bit rotational speed: field data vs. computational model response, Eq. (6), point (120 RPM, 245 kN).

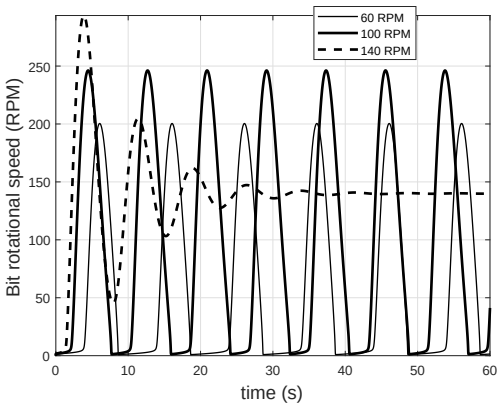

Figure 4. Bit rotational speed: field data vs. computational model response, Eq. (6), with constant top-drive speeds (60 RPM, 100 RPM, 140 RPM).

five different control strategies. The five control strategies analyzed are the following ones: (i) imposed top-drive speed, (ii) control strategy 1 (PD-control), (iii) control strategy 2 (PD-control using the weight-on-bit; only information at the top) (iv) control strategy 3 (PD-control using the weight-on-bit; with information from the bit), and (v) control strategy 4 (PD-control using the weight-on-bit and the bit response).

Figure 5 shows the stability map obtained by the model that imposes the speed at the top, Eq. (6). A 10×10 grid is considered and the contour plot represents the values of the stick-slip severity factor. The dark blue region is the stable region, where there is no torsional oscillation. The points in the regions with other colors represent responses with torsional oscillations, $SSS > 0.1$ (where 0.1 is an arbitrary tolerance). The figure shows that, for high top-drive speeds and low weight-on-bit there is less bit oscillations, and for low top-drive speeds and high weight-on-bit the oscillation is more intense.

Figure 6 shows a particular characteristics of the nonlinear system under investigation. The same equation is analyzed, Eq. (6), but while in Fig. 5 the initial speed of the simulations is $\dot{\theta}_{bit}(t=0) = 0$, in Fig. 6 the initial speed is $\dot{\theta}_{bit}(t=0) = \omega_{ref}$. It can be observed that the stability region increases when the initial condition is changed.

For the next simulations, only the worst case scenario, when $\dot{\theta}_{bit}(t=0) = 0$, is considered.

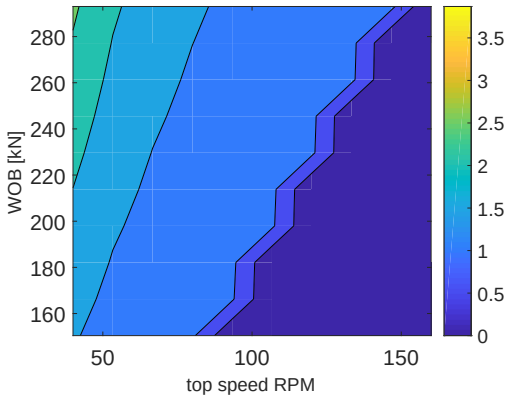

Figure 5. Stability map for imposed top-drive speed. The colors represent the values of the stick-slip severity factor.

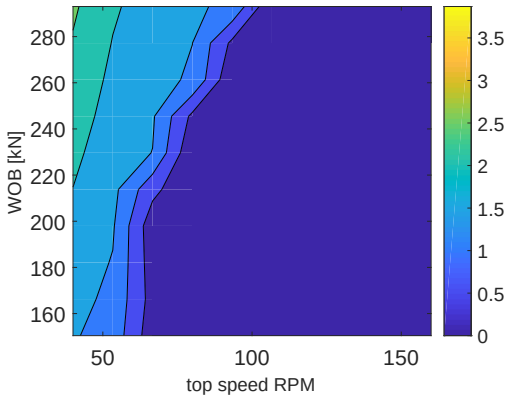

Figure 6. Stability map for imposed top-drive speed, where the initial speed in the simulations is $\dot{\theta}_{bit}(t=0) = \omega_{ref}$. The colors represent the values of the stick-slip severity factor.

Another preliminary investigation is carried out for the linearized system, around the nominal rotational speed. In this case, the stability is characterized by the eigenvalues of the linearized system matrix. Figure 7 shows the stability map for the linearized system presented in Eq. 6. For each pair (top-drive speed, weight-on-bit) the highest real part of the eigenvalues is identified. When this highest real part is positive the system is unstable (yellow region), and when it is negative the system is stable (dark blue region).

Obviously some dynamic features are missed when the system is linearized, therefore in this paper we proceed with the nonlinear time domain analysis. Nevertheless, if fast computations are needed, the linearized system could be of great value.

Let us get back to the investigation of the stability maps obtained with the different PD-control strategies depicted in the present paper. Depending on the initial guess used in the optimization algorithm, a different $\mathbf{k}$ is identified, yielding quite different results. Therefore, attention is needed because there are several local minima in the optimization problem.

Figure 8 shows the stability map obtained for the control strategy 1, Eqs. (8) and (9). Figure 8(a) shows the stability map when the initial guess is $(k_p = 10000, k_d = 100)$, and Fig. 8(b) shows the stability map when the initial guess used in the optimization algorithm is the previous identified (k_p, k_d). The best result (bigger stable region) is shown

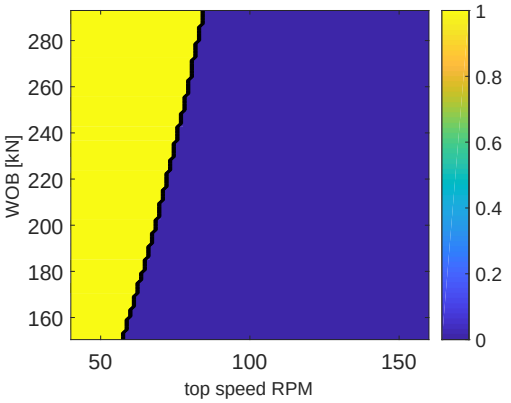

Figure 7. Stability map of the linearized system. Yellow region represents instability (at least one eigenvalue with positive real part), while the dark blue region represents stability (all eigenvalues with negative real part).

in Fig. 8(b), which yields a similar result to the previous strategy of imposed top-drive speed, Fig. 5. To tackle the problem of several minima, different initial guesses are tested, and the best stability map obtained is recorded.

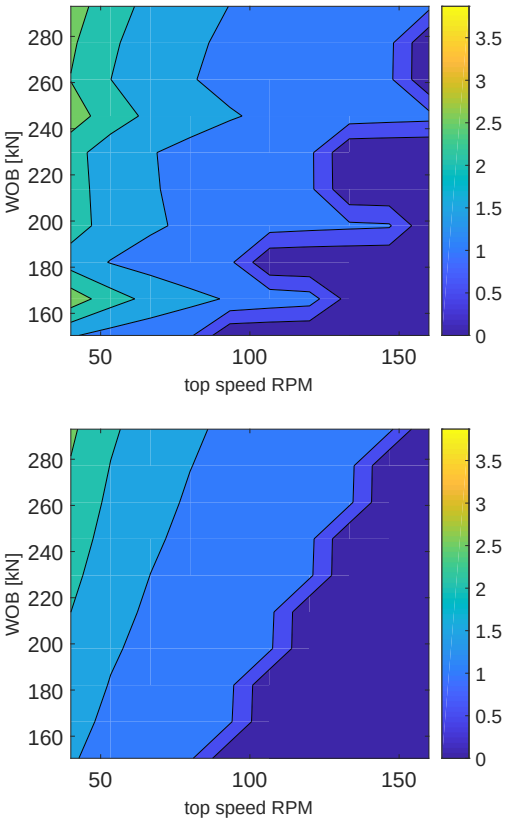

Figure 8. Stability map, PD-control strategy 1 (a) initial guess $(k_p = 10000, k_d = 100)$ (b) using previous identified (k_p, k_d) as initial guess.

Figure 9 shows the stability map obtained for the control strategy 2, Eqs. (10) and (11). And Figure 10 shows the stability map obtained for the control strategy 3, Eqs. (12) and (13), and control strategy 4, Eqs. (14) and (15).

As mention previously, the control strategy 1 yields very similar results comparing to the strategy of imposing the top-drive speed, Figs. 5 and 8(b). The control strategy 2, which includes the information about the weight-on-bit, improves significantly the results, Fig. 9. For instance, top-drive speeds above 100 RPM lead to a stable system, without stick-slip oscillations. There is also a stable region (dark blue) around 60 RPM, in the middle of two unstable regions.

Looking at the results obtained from the control strategy 3, Fig. 10(a), it can be noted that all the region under analysis is stabilized. That is, for any combination of top-drive speed and weight-on-hook, control gain coefficients that mitigate torsional oscillations were able to be identified. This means that knowing the dynamics at the bottom increases significantly the performance of the PD-control in terms of torsional vibration reduction.

The stability map obtained for the control strategy 4, Fig. 10(b), is similar to the results obtained for the control strategy 3, Fig. 10(a). We expect that the control strategy 4 performs at least as good as the control strategy 3, since the latter is a particular case of the former.

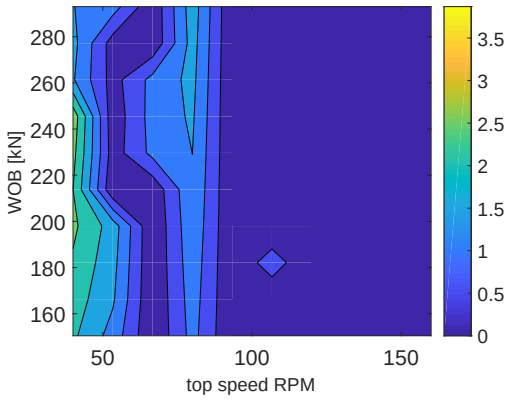

Figure 9. Stability map for PD-control strategy 2. The colors represent the values of the stick-slip severity factor.

Summarizing the results:

- The maximum value of the SSS for the four strategies was, respectively, 2.59, 3.38, 0.01, 0.01.
- Gain coefficients for the control strategy number 1:
  $k_P \sim 6.2 \times 10^4$
  $k_D \sim 900$
- Gain coefficients for the control strategy number 2:
  $k_P \sim\in [0.1 \times 10^4, 7.5 \times 10^4]$
  $k_D \sim 900$
  $k_{\mathcal{W}} \sim\in [0.1, 950]$
- Gain coefficients for the control strategy number 3:
  $k_P \sim 5.4 \times 10^4$
  $k_D \sim 950$
  $k_{\mathcal{W}} \sim\in [400, 600]$
- Gain coefficients for the control strategy number 4:
  $k_{P1} \sim [0.1 \times 10^4, 0.9 \times 10^4]$
  $k_{D1} \sim 950$
  $k_{\mathcal{W}} \sim\in [400, 600]$
  $k_{P2} \sim 0.1 \times 10^4$
  $k_{D2} \sim\in [25, 300]$

Let us emphasize some aspects of these results. For control strategy 1, for all the domain analyzed, the identified control

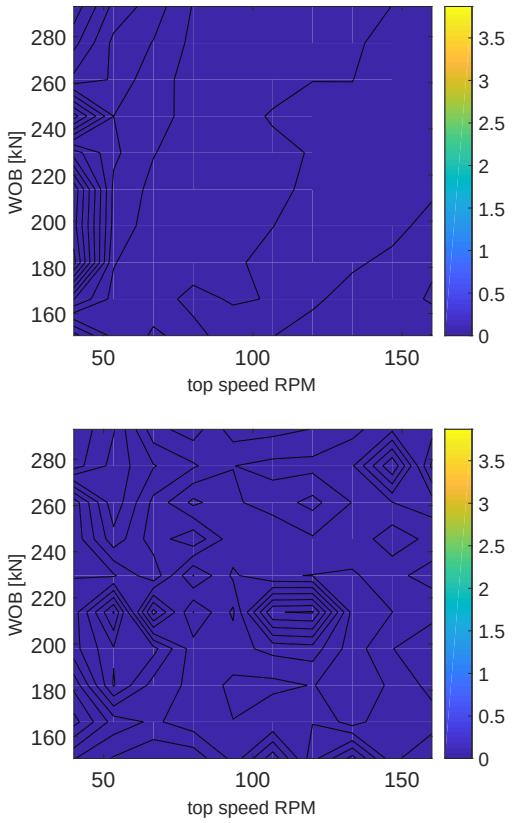

Figure 10. Stability map (a) PD-control strategy 3 and (b) PD-control strategy 4. The colors represent the values of the stick-slip severity factor.

gain coefficients are pretty much the same. For control strategy 2, another control gain $k_{\mathcal{W}}$ is included, and the proportional gain coefficient k_P might vary from about 0.1×10^4 to about 7.5×10^4 N.m, and the gain coefficient related to the weigh-on-bit varies a lot depending on the values of the reference top-drive speed and reference weight-on-bit. For control strategy 3, the proportional gain coefficient do not change much (in a level lower than the value presented for the control strategy 1), and the gain related to the weigh-on-bit varies less, comparing to the control strategy 2. Finally, for control strategy 4, two more control gain coefficients are added. This allows the proportional gain coefficient k_{P1} to assume lower values.

Concluding remarks

In the present paper, different PD-control strategies, which include controlling the weight-on-bit (or weight-on-hook) and taking into account information of the bit speed, were investigated. A simple 2DOF system is considered in the analyses. This simple system was calibrated with a 5 km drill-string field data, and seems to be representative of the phenomenon analyzed, which is torsional vibrations.

Although simple, the nonlinearity makes results quite interesting. For example, different initial conditions for the dynamics, and different initial guesses for the gain coefficients in the optimization algorithm, might lead to completely different stability maps.

Four different control strategies with increasing information required were investigated, and the control gain coefficients were obtained through optimization. It is noted that, for the system analyzed, the information of the dynamics at the bottom (bit speed) increases the performance of the PD-controller significantly in terms of torsional vibration reduction.

As future work, a multiple DOF system and uncertainties should be taken into account in order to construct a robust control strategy. The linearized system can also be investigated, using different control strategies, for instance, pole placement in the frequency domain (Ghandchi-Tehrani et al. (2013, 2015)). Especially, if many simulations are needed to generate the numerical simulations, fast computations with a linearized system could be of great value.

Acknowledgements

The second author would like to acknowledge the financial support of the Brazilian agencies CNPQ, CAPES, and FAPERJ.

References

Besselink, B., Vromen, T., Kremers, N., Van De Wouw, N.: Analysis and Control of Stick-Slip Oscillations in Drilling Systems. IEEE Transactions on Control Systems Technology, Vo. 24, No 5, 7353168, pp. 1582-1593 (2016).

Christoforou, A.P., Yigit, A.S., 2003, Fully coupled vibrations of actively controlled drillstrings, Journal of Sound and Vibration, Vo. 267, No 5, pp. 1029-1045.

Ghandchi-Tehrani, M., Wilmshurst, L.I., Elliott, S.J., 2013, Receptance method for active vibration control of a nonlinear system, Journal of Sound and Vibration, Vo. 332, No 19, pp. 4440-4449.

Ghandchi-Tehrani, M., Wilmshurst, L.I., Elliott, S.J., 2015, Bifurcation control of a Duffing oscillator using pole placement, Journal of Sound and Vibration, Vo. 21, No 14, pp. 2838-2851.

Al-Hiddabi, S.A., Samanta, B., Seibi, A., 2003, Non-linear control of torsional and bending vibrations of oilwell drillstrings, Journal of Sound and Vibration, Vo. 265, No 2, pp. 401-415.

Jansen, J.D., van den Steen, L., 1995, Active damping of self-excited torsional vibrations in oil well drillstrings, Journal of Sound and Vibration, Vo. 179, No 4, pp. 647-668.

Khulief Y.A.; Al-Sulaiman F.A.; Bashmal S., 2007, Vibration analysis of drillstrings with self excited stick-slip oscillations. Jounal of Sound Vibration, Vo. 299, pp. 540-558.

Kreuzer, E., Steidl, M., 2012, Controlling torsional vibrations of drill strings via decomposition of traveling waves, Archive of Applied Mechanics, Vo. 82, No 4, pp. 515-531.

Leine, R.I., Van Campen, D.H., Keultjes, W.J.G., 2002, Stick-slip whirl interaction in drillstring dynamics, Journal of Vibration and Acoustics, Transactions of the ASME, Vo. 124, No 2, pp. 209-220.

Liu, X., Vlajic, N., Long, X., Meng, G., Balachandran, B., 2014, Coupled axial-torsional dynamics in rotary drilling with state-dependent delay: stability and control, Nonlinear Dynamics, Vo. 78, No 3, pp. 1891-1906.

Monteiro, H.L.S., Trindade, M.A., 2017, Performance analysis of proportional-integral feedback control for the reduction of stick-slip-induced torsional vibrations in oil well drillstrings. Journal of Sound and Vibration, Vo. 398, pp. 2838.

Navarro-López, E.M., Cortés, D., 2007, Sliding-mode control of a multi-DOF oilwell drillstring with stick-slip oscillations, Proceedings of the American Control Conference, 4282198, pp. 3837-3842.

Patil, P.A., Teodoriu, C., 2013, A comparative review of modelling and controlling torsional vibrations and experimentation using laboratory setups, Journal of Petroleum Science and Engineering, Vo. 112, pp. 227-238.

Pavone, D.R., Desplans, J.P., 1994, Application of high sampling rate downhole measurements for analysis and cure of stick-slip in drilling, Proceedings - SPE Annual Technical Conference and Exhibition, Delta, pp. 335-345.

Richard, T., Germay, C., Detournay, E., 2007, A simplified model to explore the root cause of stick-slip vibrations in drilling systems with drag bits, Journal of Sound and Vibration, Vo. 305, No 3, pp. 432-456.

Ritto T.G., Gruzman M., Sampaio R., Weber H.I., 2010, Fuzzy logic control of a drill string, Proceedings of CILAMCE, Buzios (RJ), Brazil.

Ritto, T.G., Soize, C., Sampaio, R., 2009, Non-linear dynamics of a drill-string with uncertain model of the bit-rock interaction, 2009, International Journal of Non-Linear Mechanics, Vo. 44, No 8, pp. 865-876.

Ritto, T.G., Aguiar, R.R., Hbaieb, S., 2017, Validation of a drill string dynamical model and torsional stability, Meccanica, Vo. 52, No 11-12, pp. 2959-2967 .

Sampaio R, Piovan MT, Lozano GV, 2007 Coupled axial/torsional vibrations of drilling-strings by mean of nonlinear model, Mechanics Research Communication, Vol. 34, No. 5-6, pp. 497-502.

Serrarens A.F.A., Van De Molengraft M.J.G., Kok J.J., Van Den Steen L., 1998, H-infinity Control for suppressing stick-slip in oil well drillstrings, IEEE Control System Magazine, Vol .18, No 2, pp. 19-30.

Shi J., Durairajan B., Harmer R., Chen W., Verano F., Arevalo Y., Douglas C., Turner T., Trahan D., Touchet J., Shen Y., Zaheer A., Pereda F., Robichaux K., Cisneros D., 2016, Integrated efforts to understand and solve challenges in 26-in salt drilling, Gulf of Mexico. In: SPE 180349-MS, SPE Deepwater Drilling and Completions Conference, Galveston, Texas, USA

Tucker, R.W., Wang, C., 2003, Torsional vibration control and cosserat dynamics of a drill-rig assembly, Meccanica, Vo. 38, No 1, pp. 143-159.

Viguie, R., Kerschen, G., Golinval, J.-C., McFarland D.M., Bergman L.A., Vakakis, A.F., van de Wouw, N., 2009, Using passive nonlinear targeted energy transfer to stabilize drill-string systems, Mechanical Systems and Signal Processing, Vo. 23, No 1, pp. 148-169.